On the dispersion of a non-orthogonal TLM Cell

Zaiqing Li, Sandrick Le Maguer, Michel Ney

On the dispersion of a non-orthogonal TLM cell

Zaiqing Li[1], Sandrick Le Maguer[2] and Michel Ney[2,*,†]

[1]*Chinese Aeronautical Radio Electronics Research Institute (CARERI), 200233 Shanghai, China*
[2]*Laboratory of Electronics and Systems for Telecommunications (LEST, CNRS), ENST Bretagne/University of Western Brittany, CS 83818, 29238 Brest Cedex 3, France*

The numerical dispersion of a non-orthogonal transmission line matrix (TLM) algorithm is for the first time investigated. First of all, the dispersion relation is derived in the most general possible case. Then, the validation is carried out in the analysis of a simple one-dimensional example. Results show that the theory is in excellent agreement with the numerical simulation. Numerical results concerning various cell shape dispersion characteristics are presented and show some relatively weak numerical dispersion even for rather highly distorted cells. Finally, some indications concerning cell shape selection to minimize the non-orthogonal TLM cell are proposed.

KEY WORDS: TLM; time domain; non-orthogonal cell; numerical dispersion

1. INTRODUCTION

The accuracy of the transmission line matrix (TLM) modeling scheme depends on various factors, such as mesh coarsness, time truncation and numerical dispersion. The latter is characterized by the wave velocity error produced by the numerical model (discrete medium) compared with the real velocity that occurs in the corresponding physical (homogenous) medium. The dispersion error depends on various factors, such as the medium parameters, the wave direction of propagation relatively to the mesh axis, the mesh size and the time step. As a result, a complete dispersion analysis is a difficult task. In addition, an analytical solution for dispersion characteristic is possible only for infinite mesh with identical cells. Therefore, only restricted cases that fulfill these conditions can be tackled in the case of non-orthogonal cells. However, even for limited cases, the dispersion analysis of a numerical scheme allows one to extract useful information to minimize dispersion error, such as cell geometry, time step, etc.

*Correspondence to: Michel Ney, Laboratory of Electronics and Systems for Telecommunications (LEST, CNRS), ENST Bretagne/University of Western Brittany, CS 83818, 29238 Brest Cedex 3, France.
†E-mail: Michel.Ney@enst-bretagne.fr

Some intense work has been carried out on the dispersion of TLM algorithm. For instance, the well-known symmetrical condensed node (SCN) was thoroughly analyzed [1, 2].

A general dispersion relation for unloaded node (without stubs) was derived under the form of an eigenvalue equation. Solutions were also found [3, 4] for the super SCN (SSCN) [5]. Some subsequent work concerns extension of dispersion analysis to orthogonal SCN cell loaded with stubs [6–17]. In particular, a dispersion relation was derived based on a field representation in Hilbert space [15–17]. Finally, dispersion relation for non-orthogonal TLM cells proposed by Hein [18, 19] has not been yet published in detail. This subject constitutes the objective of this paper.

2. THE DISPERSION RELATION OF A NON-ORTHOGONAL TLM

Let us consider an infinite mesh composed of identical cells. To fulfill the constraint related to dispersion analysis, these cells need not be orthogonal, i.e. parallel to Cartesian axes, but should have parallel tilted faces (see Figure 1). As a result, such a mesh constitutes a periodically loaded medium of infinite extent. Now, consider an ordinary plane wave propagating in such a medium. The TLM mechanism uses arm voltages to propagate fields in the mesh. At $(n-\frac{1}{2})\Delta t$ (Δt being the time step), voltages are incident on the node. Voltages propagate in the node arms scatter and produce reflected voltages at $(n+\frac{1}{2})\Delta t$. If $\mathbf{a}^{n-1/2}$ and $\mathbf{b}^{n+1/2}$ are the reflected and incident node voltage vectors, respectively, the scattering process at every node can be expressed as

$$\mathbf{b}^{n+1/2} = \mathbf{S}\mathbf{a}^{n-1/2} \tag{1}$$

where $n+1/2$ and $n-1/2$ are discrete time indexes and $\mathbf{S}$ the 18×18 TLM node scattering matrix that is generally composed of 12 ports and six stubs. Then, there exists a relationship between reflected voltages at $n+1/2$ and $n-1/2$

$$\mathbf{b}^{n-1/2}\mathbf{T} = \mathbf{b}^{n+1/2} \tag{2}$$

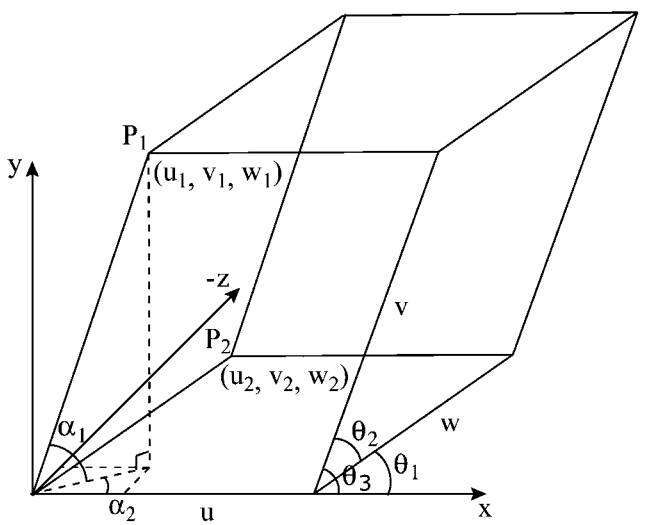

Figure 1. Non-orthogonal TLM cell.

where

$$\mathbf{T} = T_0\mathbf{I} \tag{3}$$

and for a wave of angular frequency ω, $T_0 = \mathrm{e}^{-\mathrm{j}\omega\Delta t}$, where $\mathbf{I}$ is the unity matrix.

Hence, one can derive a relationship between reflected and incident voltages at the same time index:

$$\mathbf{b}^n = \mathbf{TSa}^n \tag{4}$$

At this stage, one can take into account the transfer relationship between neighboring cells. It includes the discrete space shift between cells and constitutes a second relationship between incident and reflected voltages at time index n:

$$\mathbf{a}^n = \mathbf{P}'\mathbf{b}'^n = \mathbf{P}\mathbf{b}^n \tag{5}$$

where $\mathbf{P}'$ is the transfer matrix between neighboring cells, $\mathbf{b}'^n$ the neighboring cell access voltage vector and $\mathbf{P}$ the connection matrix that represents the transfer relation of access voltages, including spatial shift as illustrated in Figure 2.

At time index n, neighboring cell reflected voltage b'_{11} becomes the incident voltage a_3. At the same time, there exists a simple relationship between b'_{11} and b_{11}:

$$b'_{11} = \mathrm{e}^{-\mathrm{j}\mathbf{k}\cdot\Delta\mathbf{r}}b_{11} \tag{6}$$

The above relations can be summarized as follows:

$$a_3^n = b_{11}'^n = \mathrm{e}^{-\mathrm{j}\mathbf{k}\cdot\Delta\mathbf{r}}b_{11}^n = P_{3,11}b_{11}^n \tag{7}$$

where $\mathbf{k}$ is the wave vector, $\Delta\mathbf{r}$ is the vector along the path shown in Figure 2 and $P_{3,11}$ the $\mathbf{P}$ matrix element located at the third row and 11th column. Hence, one can write

$$P_{3,11} = \mathrm{e}^{-\mathrm{j}\mathbf{k}\cdot\Delta\mathbf{r}} \tag{8}$$

The complete determination of the matrix $\mathbf{P}$ will be carried out as explained above. Details will follow later. From (4) and (5), one obtains

$$\mathbf{a}^n = \mathbf{PTSa}^n \tag{9}$$

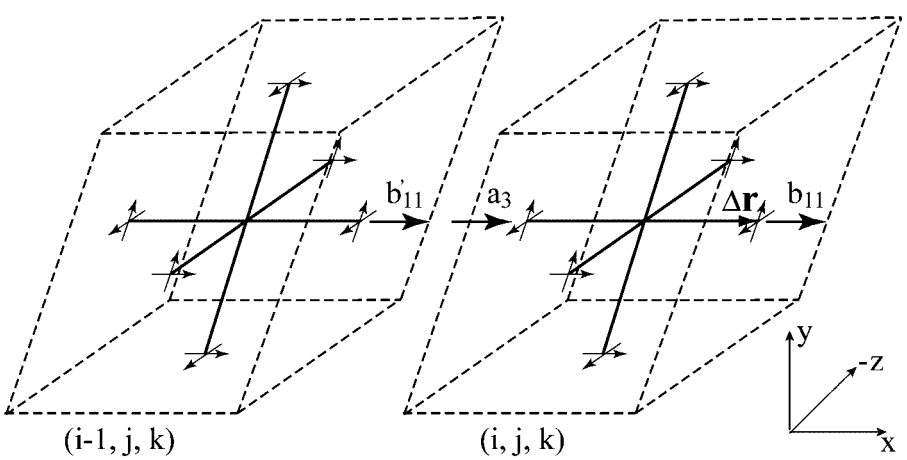

Figure 2. Voltage transfer between neighboring cells.

or equivalently the eigenvalue matrix equation:

$$(\mathbf{PTS} - \mathbf{I})\mathbf{a}^n = 0 \tag{10}$$

Note that according to (3), one has

$$\mathbf{PTS} = \mathbf{TPS} \tag{11}$$

Thus, by using the definition of **T**, (10) becomes

$$(\mathbf{PS} - \mathrm{e}^{-\mathrm{j}\zeta}\mathbf{I})\mathbf{a}^n = 0 \tag{12}$$

where ζ is the phase shift defined by $\zeta = \omega\Delta t$. Therefore, eigenvalues are obtained by finding roots of the polynomial generated by the determinant

$$\det(\mathbf{PS} - \mathrm{e}^{-\mathrm{j}\zeta}\mathbf{I}) = 0 \tag{13}$$

This constitutes the non-orthogonal TLM node dispersion relation under the assumption of identical cells in the infinite mesh. It has the same form as for other TLM nodes except that **P** and **S** have different components.

Now, scattering matrix **S** and connection matrix **P** remain to be determined. First of all, geometrical node vector $\mathbf{B}_i$ and surface vector $\mathbf{A}_i$ have to be evaluated (see Figure 3). By considering quantities illustrated in Figure 1, it can be noted that if $u, v, w, \theta_1, \theta_2$ and θ_3 are known, the various angles are related in a spherical coordinate system:

$$\cos\theta_3 = \cos\alpha_1 \cos\alpha_2 \tag{14}$$

$$\cos\theta_2 = \cos\alpha_1 \cos(\theta_1 - \alpha_2) \tag{15}$$

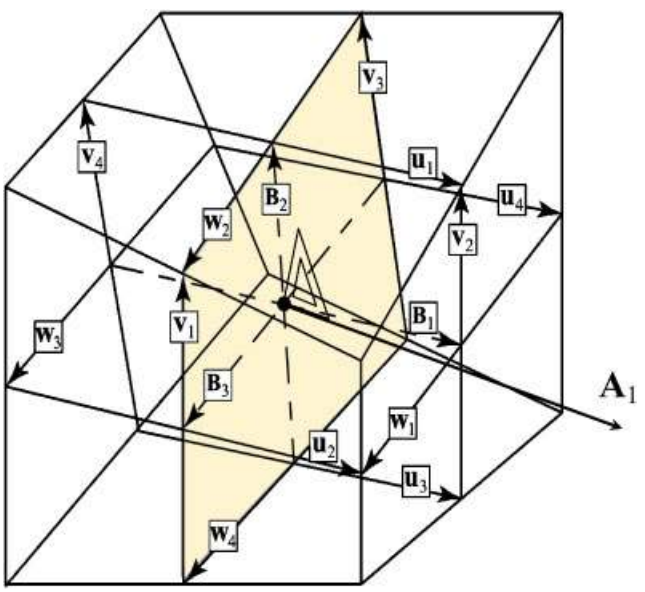

Figure 3. Illustration of node vector $\mathbf{B}_i$ and surface vector $\mathbf{A}_1$ [18].

from which one can deduce

$$\alpha_1 = \arccos \frac{\cos^2\theta_2 - 2\cos\theta_1\cos\theta_2\cos\theta_3 + \cos^2\theta_3}{\sin\theta_1} \tag{16}$$

$$\alpha_2 = \arctan \frac{\cos\theta_2 - 2\cos\theta_1\cos\theta_3}{\sin\theta_1\cos\theta_3} \tag{17}$$

P_1 and P_2 have Cartesian coordinates as follows:

$$\begin{bmatrix} u_1 = v\cos\theta_3 \\ v_1 = v\sin\alpha_1 \\ w_1 = -\sqrt{v^2 - u_1^2 - v_1^2} \end{bmatrix} \quad \text{and} \quad \begin{bmatrix} u_2 = w\cos\theta_1 \\ v_2 = 0 \\ w_2 = w\sin\theta_1 \end{bmatrix} \tag{18}$$

Vectors $\mathbf{B}_i$ and $\mathbf{A}_i$ $(i = 1, 2, 3)$ are generally expressed by [18]:

$$\mathbf{B}_i = \sum_{v=1}^{4} \mathbf{s}_i^v, \quad \mathbf{s}_i \in \{\mathbf{u}, \mathbf{v}, \mathbf{w}, \} \tag{19}$$

$$\mathbf{A}_1 = \frac{1}{4}\sum_{v,\mu} \mathbf{v}^v \times \mathbf{w}^\mu \quad (v = 1, 3; \mu = 2, 4) \tag{20}$$

Thus, according to the geometry of Figure 1 and (18), the above vectors become

$$\begin{gathered} \mathbf{B}_1 = 4u\mathbf{e}_x, \quad \mathbf{A}_1 = u_1w_2\mathbf{e}_x - (u_2w_1 + u_1w_2)\mathbf{e}_y + u_2v_1\mathbf{e}_z \\ \mathbf{B}_2 = 4u_1\mathbf{e}_x + 4v_1\mathbf{e}_y + 4w_1\mathbf{e}_z, \quad \mathbf{A}_2 = uw_2\mathbf{e}_y \\ \mathbf{B}_3 = -4u_2\mathbf{e}_x + 4w_2\mathbf{e}_z, \quad \mathbf{A}_3 = -uw_1\mathbf{e}_y + uv_1\mathbf{e}_z \end{gathered} \tag{21}$$

where $\mathbf{e}_x$, $\mathbf{e}_y$ and $\mathbf{e}_z$ are the Cartesian unit vectors. Hence, one completely defines the geometry of the non-orthogonal cell by the matrices:

$$B = \begin{bmatrix} 4u & 4u_1 & -4u_2 \\ 0 & 4v_1 & 0 \\ 0 & 4w_1 & 4w_2 \end{bmatrix}, \quad A = \begin{bmatrix} u_1w_2 & 0 & 1 \\ -(u_2w_1 + u_1w_2) & uw_2 & -uw_1 \\ u_2v_1 & 1 & uv_1 \end{bmatrix} \tag{22}$$

From the above matrices, the node scattering matrix $\mathbf{S}$ can be determined. Also, from the matrix B expressed in (22), the connection matrix $\mathbf{P}$ elements can be determined

$$\begin{gathered} P_{1,12} = P_{5,7} = \mathrm{e}^{\mathrm{j}\mathbf{k}\cdot\mathbf{B}_2/4} = \mathrm{e}^{\mathrm{j}(k_xu_1 + k_yv_1 + k_zw_1)}, \quad P_{9,2} = P_{8,4} = \mathrm{e}^{-\mathrm{j}\mathbf{k}\cdot\mathbf{B}_3/4} = \mathrm{e}^{\mathrm{j}(k_xu_2 - k_zw_2)} \\ P_{12,1} = P_{7,5} = \mathrm{e}^{-\mathrm{j}\mathbf{k}\cdot\mathbf{B}_2/4} = \mathrm{e}^{-\mathrm{j}(k_xu_1 + k_yv_1 + k_zw_1)}, \quad P_{3,11} = P_{6,10} = \mathrm{e}^{-\mathrm{j}\mathbf{k}\cdot\mathbf{B}_1/4} = \mathrm{e}^{\mathrm{j}k_xu} \\ P_{2,9} = P_{4,8} = \mathrm{e}^{\mathrm{j}\mathbf{k}\cdot\mathbf{B}_3/4} = \mathrm{e}^{\mathrm{j}(-k_xu_2 + k_zw_2)}, \quad P_{11,3} = P_{10,6} = \mathrm{e}^{-\mathrm{j}\mathbf{k}\cdot\mathbf{B}_1/4} = \mathrm{e}^{-\mathrm{j}k_xu} \end{gathered} \tag{23}$$

where $\mathbf{k}$ is the free space wave vector. Finally, reflected voltages on the six stubs come back to the nodes. Hence,

$$P_{13,13} = P_{14,14} = P_{15,15} = 1, \quad P_{16,16} = P_{17,17} = P_{18,18} = 1 \tag{24}$$

All other matrix elements are zero.

As seen before, the dispersion problem leads to the eigenvalue problem (12). For orthogonal nodes, it is possible to find analytical solutions in certain cases, such as unloaded SCN and cubic SSCN. Other cases lead to complex expression to solve, in particular non-cubic cell and/or operation at arbitrary time steps smaller than the maximum allowed value ($\Delta t_{\max}$) that insures stability. In the case of non-orthogonal TLM cell, 12 lines and six stubs are involved and expressions (12) and (13) are rather involved. Consequently, it is simpler to use a numerical procedure for solutions.

3. TYPES OF SOLUTION

Although no analytical solutions will be given, a preliminary qualitative analysis is necessary to extract the types of solutions expected. In (13) **S** and **P** are 18×18 matrices. Thus, the left-hand side of (13) can be written as a 18th-order polynomial and (12) can be expressed as follows:

$$\sum_{i=0}^{18} B_i \lambda^{18-i} = 0 \tag{25}$$

where $\lambda = e^{-j\zeta}$. Hence, there will be 18 eigenvalues $\lambda_i = e^{-j\zeta_i}$ that correspond to various possible modes. These modes can be classified into four major categories [1, 8]:

(1) $\lambda = 1$ or $\zeta = 0$: Eigenvalues corresponding to non-propagating modes and representing electro- and magneto-static cases.
(2) $\lambda = -1$ or $\zeta = \pi$: Eigenvalues corresponding to non-propagating modes and representing non-physical solutions oscillating at frequency, $f = 1/(2\Delta t)$.
(3) $\zeta < \pi/2$: Eigenvalues corresponding to physical modes at low frequency.
(4) $\zeta \geqslant \pi/2$: Eigenvalues corresponding to physical modes at high frequency.

Among the above types of solutions, dispersion analysis is concerned only by dynamic modes, i.e. solutions of types 3 and 4. In addition, high-frequency solutions are located beyond the TLM model validity. Consequently, one shall consider only type 3 solutions.

4. VALIDATION

In (13), matrix **P** elements (23) are related to the wave vector **k** (see Figure 4). Knowing **k**, ϕ, ψ, the vector components are given by

$$\begin{aligned} k_y &= k \cos\theta \\ k_x &= \sqrt{k^2 - k_y^2} \sin\psi \\ k_z &= \sqrt{k^2 - k_x^2 - k_y^2} \end{aligned} \tag{26}$$

where k is the magnitude of the vector **k**. Now, suppose an isotropic medium with arbitrary relative permittivity and relative permeability ε_r and μ_r, respectively. Thus, $k = 2\pi/\lambda$, where λ is the medium (known) physical wavelength. Consequently, for such a medium, one can completely determine the numerical values involved in the eigenvalue equation (13) with the exception of ζ_i values, which are to be found numerically.

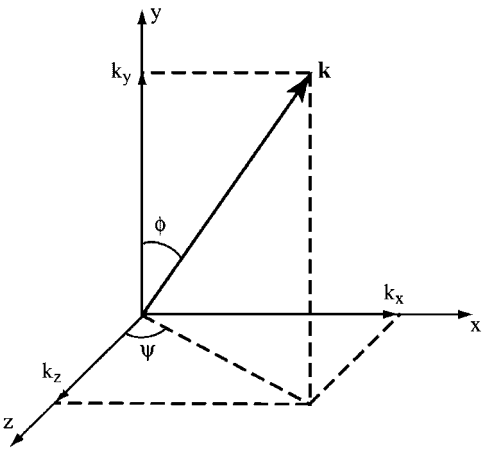

Figure 4. Wave vector components.

For comparison, one has to determine the wave propagation factor $\tilde{k}$ (which corresponds to the phase velocity $\tilde{c} = \tilde{c}_0/\sqrt{\mu_r \varepsilon_r}$) given by the TLM model. Selected solutions ($\zeta_i \geqslant \pi/2$) are related to the numerical wave propagation factor as

$$\zeta = \omega \Delta t = \tilde{k} c \Delta t \tag{27}$$

where c is the medium speed of light. Consequently, since the medium is known and the time step fixed, the numerical wave propagation factor can be computed for each case (cell geometry, medium, wave incidence and Δt) from the eigenvalues and using (27):

$$\tilde{k} = \frac{\zeta_i}{c\Delta t} = \frac{\zeta_i \sqrt{\mu_r \varepsilon_r}}{c_0 \Delta t} \tag{28}$$

Note that one selects the wave vector value by taking into account the usual limit of acceptable dispersion of the TLM $\Delta l/\lambda \sim 0.1$, where Δl is the maximum size of the cell. Finally, the relative error on the wave propagation factor is defined here by

$$\delta k' = \frac{\tilde{k} - k}{k} \tag{29}$$

It has been shown that all condensed TLM schemes have a second-order accuracy [20, 21]. As a result, one can evaluate the relative error δk corresponding to a wavelength λ from (29) established for λ':

$$\delta k = \delta k' \left(\frac{\lambda'}{\lambda} \right)^2 \tag{30}$$

If one wishes to compare or validate the dispersion results with those obtained from TLM simulation using the same non-orthogonal cells, the number of geometry cases to be tested is quite limited. The reason, stated before, concerns the assumption on infinite mesh of identical cells for dispersion analysis. Hence, a one-dimensional mesh extending to the direction of the propagating wave to be simulated is chosen. The boundary conditions on lateral planes are PECs perpendicular to the y-axis and PMCs to the z-axis (see Figure 5). That configuration defines a plane wave linearly polarized along the y-axis. The free-cell geometric parameters are the

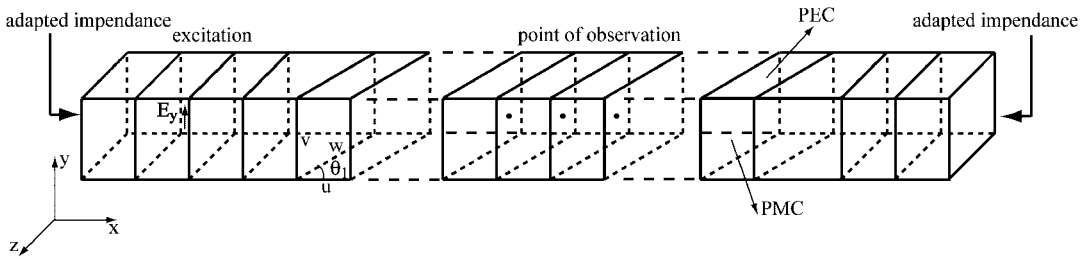

Figure 5. One-dimensional TLM mesh for theoretical dispersion results validation.

angle θ_1 and the cell dimensions (u, v, w). Finally, matching conditions must be applied to terminate the computational domain. This can be easily achieved in TLM when orthogonal cells are used. However, for the general cases considered here more complicated conditions should be developed which is not the objective of the paper. The idea is to insert few orthogonal cells at both ends of the mesh so that simple medium intrinsic impedance is used as termination to achieve a perfect match. Since the velocity error is computed in the mesh zone where non-orthogonal cells are present (see Figure 5), only some negligible effect on results is expected. Several simulations were carried out and excellent agreement between both approaches was found.

However, some slight discrepancies occur for non-equilateral cells. For instance, Figure 6 shows theoretical results obtained from numerically solving (13) and relative error computed from (30) for different angles of θ_1. Simulation results are obtained by the procedure described above that extracts the velocity error from observation point indicated in Figure 5. One can still observe some good agreement between both approaches. This also validates the assumption that the insertion of few orthogonal cells to perfectly match both ends of the TLM mesh for numerical experiments does not affect the results significantly. Also, one can already note the excellent behavior of the non-orthogonal TLM node, since at the usual limit of TLM model ($\Delta l/\lambda \sim 0.1$), the dispersion error is below 2% yet the cell is significantly distorted ($\theta_1 = 30^\circ$). However, some other experiments need to be carried out to ascertain this concluding remark. Finally, one can note that the dispersion occurs with a negative sign, which is opposite to the behavior of the standard orthogonal SCN.

5. NUMERICAL ANALYSIS OF DISPERSION

As the numerical procedure to solve the dispersion eigenequation was validated, it will be used for the solutions presented further. One shall always respect the empirical condition $\Delta l_{\max}/\lambda = 0.1$ for minimum dispersion to which a relative wave propagation error noted $\overline{\delta k}$ corresponds. This dispersion limit condition will prevail unless mentioned otherwise in the simulations. Finally, note that since the theoretical procedure is applied mentioning of the mesh and boundary is not necessary as it implies the theoretical situation of an infinite mesh of identical cells.

5.1. Tilted cells in one direction only

To extract some trend of the dispersion, one shall first investigate the simple case of a cell with faces parallel to the plane yOz only to be tilted. Hence, the inclination angle θ_1 varies from 10 to

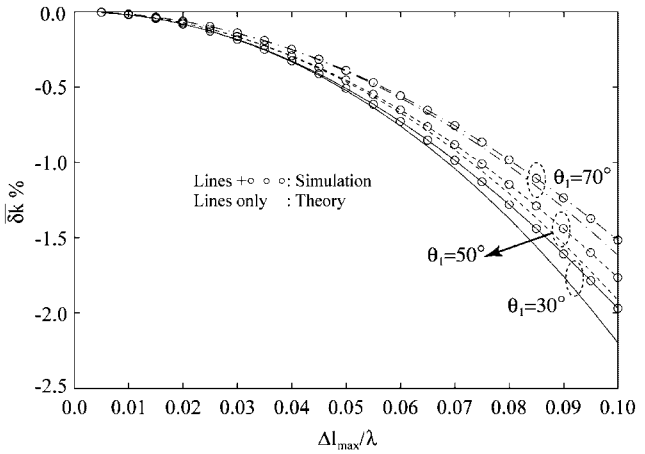

Figure 6. Relative error comparison between theory and numerical simulations ($u = 1.5v = 1.5w$).

90° while θ_2 and θ_3 remain fixed at 90°. Note that θ_1 is limited to a minimum value of 10°. The reason is that cell distortion below that value is practically never encountered. In addition, $\theta_1 = 0^\circ$ is a singular value for dispersion and for low angle values some numerical problem may arise. The propagation angle θ is varied while the angle ϕ is kept at 90° (wave vector in the plane xOz). Finally, the characteristic parameters of the medium are also varied. In addition, maximum time step is used so that the normalized time step

$$\delta t = \Delta t / \Delta t_{\max} \tag{31}$$

is unity, where $\Delta t_{\max}$ is the maximum time step that can be used for stable TLM operation. Finally, the cell dimension is fixed such as $u = v = w = u_0$.

The first case illustrated in Figure 7 is for $\varepsilon_r = \mu_r$ as this condition is often used for dispersion analysis of orthogonal cells since it simplifies dispersion equations. It was found that one single mode solution is obtained (no degeneration). Note that for an angle θ_1 small (cell maximum distortion), the error remains small of the order of 1%. The $\theta_1 = 90^\circ$ case corresponds to orthogonal SCN cell and is shown for comparison. It is clearly observed that dispersion increases as the angle θ_1 decreases. However, one has to mention that the maximum time step must be decreased as well. Thus, this also contributes to increase dispersion.

The next case whose results are shown in Figure 8 is more general as $\varepsilon_r \neq \mu_r$. Two propagating modes are possible and correspond to TE and TM cases, respectively [16]. One can observe that the relative error is always negative and that the evolution in function of θ_1 differs from the case of Figure 7. In addition, error can reach values as high as 3%. Note that this tendency is also observed for orthogonal cells (curve $\theta_1 = 90^\circ$ in Figure 8) due to the high permittivity value. On the other hand, the TM mode is slightly less dispersive, typically below 2% and its error behaves similar to the case $\varepsilon_r = \mu_r$ illustrated in Figure 7. The objective of the previous case was to observe the influence of high permittivity values. Simulations were carried out for the case of high permeability values. For instance, errors (not shown here) for $\mu_r = 4$ have some similar behavior to the ones for high permittivity values. However, the relative error was slightly smaller for the TE mode.

Another case, illustrated in Figure 9, is when both ε_r and μ_r have high values but are different. The trend is the same as the cases treated before, for both modes. However, the error is slightly

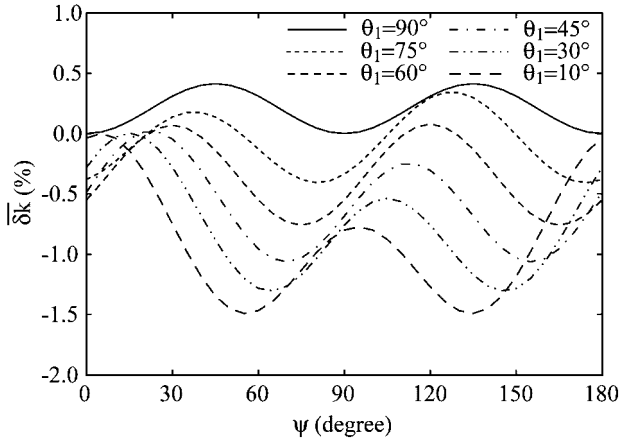

Figure 7. TLM non-orthogonal cell propagation error. Case: $\varepsilon_r = \mu_r$, $\theta_2 = \theta_3 = \phi = 90^\circ$.

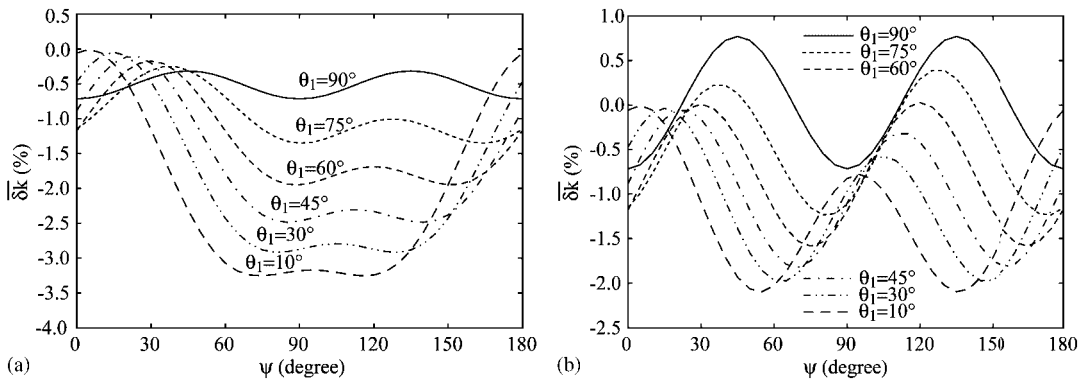

Figure 8. TLM non-orthogonal cell propagation error. Case: $\varepsilon_r = 9$, $\mu_r = 1$, $\theta_2 = \theta_3 = \phi = 90^\circ$: (a) TE mode and (b) TM mode.

smaller for the TE mode (less than 2.5%). This can be explained by a slightly higher value of the maximum time step, which contributes to decrease the dispersion.

From the above results, one can conclude that the dispersion is less severe than expected. Indeed, for cell geometry severely distorted compared with orthogonal (cubic) case the wave propagation factor relative error is below 3% at the TLM model limit ($\Delta l_{max}/\lambda = 0.1$) and maximum time step. However, it seems that the contribution to the dispersion is rather due to the decrease in the maximum time step compared with the orthogonal case than to the geometrical distortion of the cells. More complex geometry is now analyzed to confirm the above conclusion.

5.2. General geometry case with equilateral dimensions

One shall consider the case illustrated by Figure 10(a) for which all cell faces are tilted, for $\varepsilon_r = \mu_r$ and arbitrary wave direction of propagation. Other parameters are the same as for the

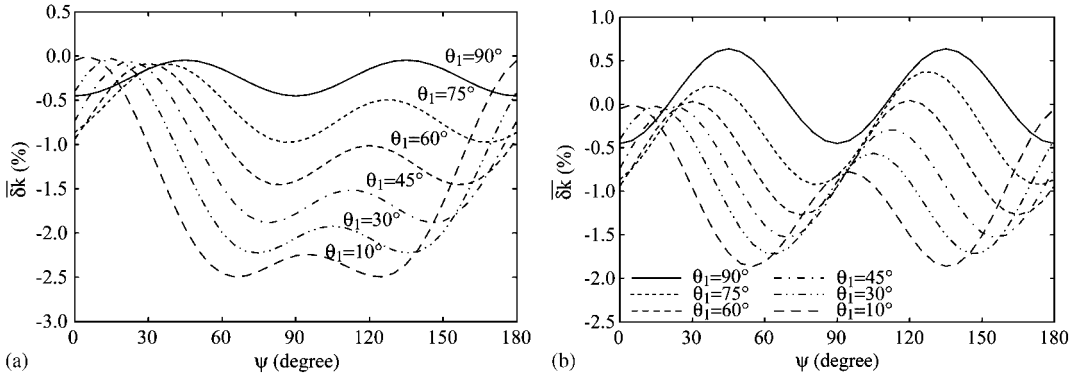

Figure 9. TLM non-orthogonal cell propagation error. Case: $\varepsilon_r = 9$, $\mu_r = 4$, $\theta_2 = \theta_3 = \phi = 90^\circ$: (a) TE mode and (b) TM mode.

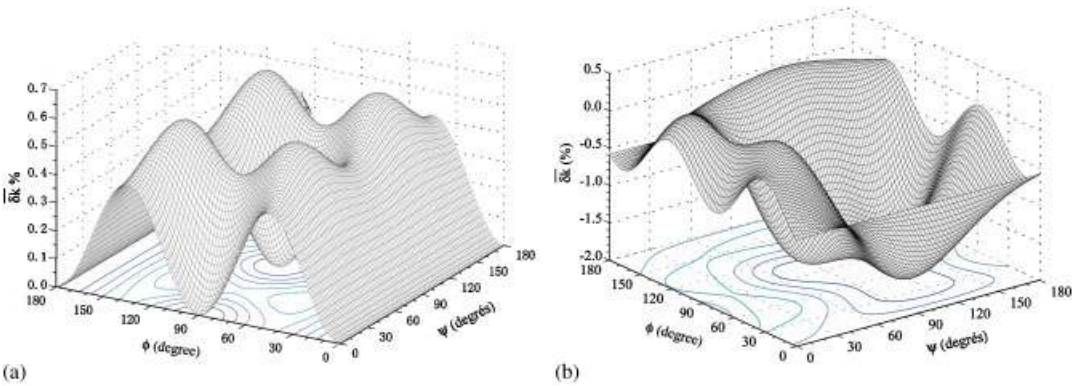

Figure 10. TLM equilateral non-orthogonal cell propagation error: (a) orthogonal case and (b) case: $\varepsilon_r = \mu_r = 1$, $\theta_1 = \theta_2 = \theta_3 = 45^\circ$.

case treated under Section 5.1. Figure 10(a) is the orthogonal case (cubic SCN) shown for reference. It has been shown that maximum dispersion for cubic orthogonal SCN occurs for propagation along diagonal directions. Figure 10(b) shows the case for all faces tilted at 45°. It can be observed that the dispersion is still very well restricted to values below 2% and, hence, confirms the excellent performance of the non-orthogonal cell. Several experiments carried out with different geometrical values (not shown) produce comparable results.

5.3. Non-equilateral cells

Dispersion analyses for the orthogonal SCN have shown that non-parallelepipedic cells exhibit higher velocity error compared with the cubic case. Thus, several numerical experiments have been carried out to investigate the influence of the cell dimensions (u, v, w). Figure 11 shows two typical situations in which only the angle θ_1 is modified. In Figure 11(a), the behavior is similar to what was observed in Figure 7 except that the dispersion is larger since the relative propagation error can reach 3% for the case $\theta_1 = 10^\circ$. This can be explained by the fact that the

time step is principally determined by the dimension v, which is smaller than for other dimensions. Also, one notes that maximums occur for both cell diagonal directions in the analysis plane. These two maximums get closer as θ_1 increases. This could be expected as fields are always computed at the cell center faces. In Figure 11(b), the plane of analysis is maintained but the dimension w is smaller than the others this time. On can note a different behavior with an increase in the relative error up to 6% for $\theta_1 = 10^\circ$. Yet, for reasonable geometry distortion, $\theta_1 \geqslant 30^\circ$, the error remains at the same level. This fact is still observed for arbitrary wave propagation angle as shown in Figure 12.

The above numerical experiments lead us to conclude that non-equilaterality remains a major factor for increasing dispersion. This has already been observed in the case of the orthogonal SCN dispersion. This is explained by a corresponding decrease in the maximum time step. The non-orthogonality of the cell enhances the effect but does not seem to play a major role in dispersion increase, except the slight reduction in the maximum time step.

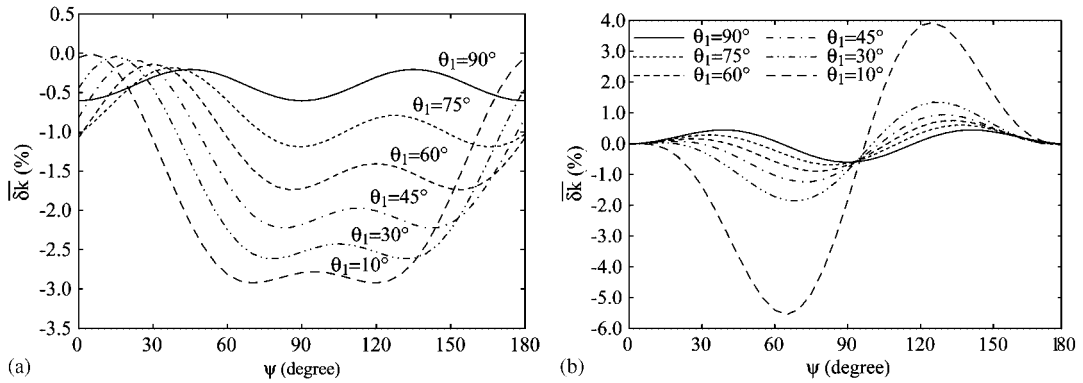

Figure 11. TLM non-equilateral, non-orthogonal cell propagation error: (a) case: $u = u_0$, $v = u_0/2$, $w = u_0$, $\varepsilon_r = \mu_r = 1$, $\theta_2 = \theta_3 = \phi = 90^\circ$ and (b) case: $u = v = u_0$, $w = u_0/2$, $\varepsilon_r = \mu_r = 1$, $\theta_2 = \theta_3 = \phi = 90^\circ$.

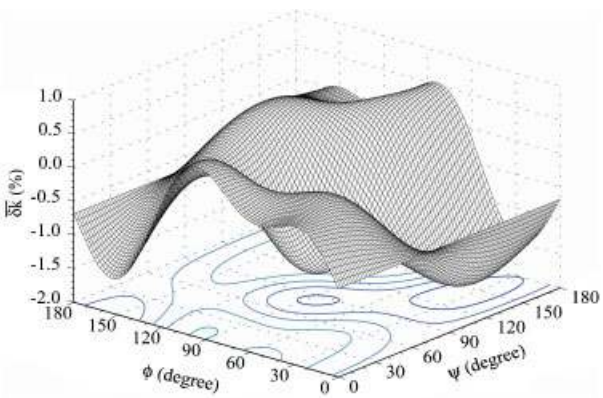

Figure 12. TLM non-equilateral, non-orthogonal cell propagation error: case: $u = v = u_0$, $w = u_0/2$, $\varepsilon_r = \mu_r = 1$, $\theta_1 = 60^\circ$, $\theta_2 = 45^\circ$, $\theta_3 = 70^\circ$.

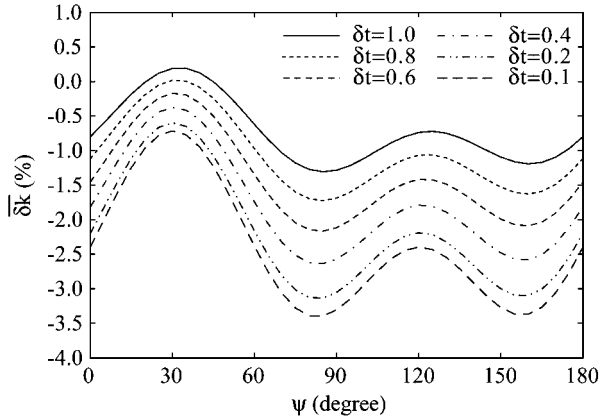

Figure 13. TLM non-equilateral, non-orthogonal cell propagation error: case $\varepsilon_r = \mu_r = 1$, $\theta_1 = 60^\circ$, $\theta_2 = 70^\circ$, $\theta_3 = 50^\circ$, $\phi = 90^\circ$.

5.4. Time-step effect

It was mentioned that time step has some impact on dispersion. With SCN, it is always recommended to use the maximum time step for which dispersion is minimized. There is no stability hazard as TLM is inherently stable even at the time step limit. However, when using non-orthogonal equilateral cells, the maximal time step is slightly reduced. As a result, this must be accompanied by some dispersion increase relatively to cubic SCN. Previous numerical experiments have shown that the increase remains small if maximum time step operation is maintained. Series of experiments were carried out to extract additional information about time step reduction effect on dispersion for the non-orthogonal cell.

Figure 13 shows a typical result for an equilateral cell for different normalized time steps. The cell geometry is fixed as well as the propagation direction. The effect is readily seen from Figure 13 as some substantial degradation is observed. Hopefully, δt remains close to unity, even for greatly distorted cells as long as they are equilateral. These observations remain valid for other numerical experiments (not shown here) involving other parameter values and for which the maximum error value remains around 3.5%.

6. CONCLUSION

The dispersion characteristic of a non-orthogonal TLM cell was thoroughly investigated. The derivation of the dispersion relation was presented in detail and leads to an eigenvalue problem. Relevant solutions corresponding to propagating modes in the frequency range where TLM model is valid were identified. The complexity of the matrix equation precludes analytical solutions for dispersion. Instead, a numerical approach was used and validated by a numerical experiment.

Simulation results show that the non-orthogonal TLM cell has some excellent behavior, especially when one considers equilateral cells. In this case, even when severe geometrical distortion is applied, the propagation relative error reaches maximum values that are about 2% higher than the classic orthogonal SCN. Noteworthy to mention that all experiments were

performed at the usual limit ($\Delta l_{\max}/\lambda = 0.1$) of the TLM model, where the dispersion is maximum.

Finally, as observed for SCN (parallelepipedic case), the model accuracy degrades when non-equal dimensions of the sides are used. It is explained by the fact that the maximum time step must be further reduced in this case, thus contributing to TLM dispersion increase.

REFERENCES

1. Nielsen JS, Hoefer WJR. A complete dispersion analysis of the condensed node TLM mesh. *IEEE Transactions on Magnetics* 1991; **27**(5):3982–3985.
2. Nielsen JS, Hoefer WJR. Generalized dispersion analysis and spurious modes of 2-D and 3-D TLM formulations. *IEEE Transactions on Microwave Theory and Techniques* 1993; **41**(8):1375–1384.
3. Krumpholz M, Russer P. On the dispersion in TLM and FDTD. *IEEE Transactions on Microwave Theory and Techniques* 1994; **42**(7):1275–1279.
4. Trenkic V, Benson TM, Christopoulos C. Dispersion analysis of a TLM mesh using a new scattering matrix formulation. *IEEE Microwave and Guided Wave Letters* 1995; **5**(3):79–80.
5. Trenkic V, Christopoulos C, Benson TM. Dispersion analysis of TLM symmetrical super-condensed node. *Electronics Letters* 1994; **30**(25):2151–2153.
6. Johns DP, Christopoulos C. Dispersion of the time-domain and frequency domain formulations of the symmetrical condensed TLM node. *Second International Conference on Computation in Electromagnetics* 1994; 295–298.
7. Celuch-Marcysiak M. Toward better understanding of the SCN TLM method for inhomogeneous problems. *Second International Workshop on Discrete Time Domain Modeling of Electromagnetics Fields and Networks*, Berlin, Germany, 1993.
8. Celuch-Marcysiak M, Gwarek WK. On the effect of bilateral dispersion in in-homogeneous symmetrical condensed node modeling. *IEEE Transactions on Microwave Theory and Techniques* 1994; **42**(6):1069–1073.
9. Trenkic V, Christopoulos C, Benson TM. Dispersion of TLM condensed nodes in media with arbitrary electromagnetic properties. *IEEE International Microwave Symposium Digest* 1995; **2**:373–376.
10. Trenkic V, Christopoulos C, Benson TM. Analytical expansion of the dispersion relation for TLM condensed nodes. *IEEE Transactions on Microwave Theory and Techniques* 1996; **44**(12):2223–2230.
11. Berini P, Wu K. A comprehensive study of numerical anisotropy and dispersion in 3-D TLM meshes. *IEEE Transactions on Microwave Theory and Techniques* 1995; **43**(5):1173–1181.
12. Morente JA, Gimenez G, Porti A, Khalladi M. Dispersion analysis for TLM mesh of symmetrical condensed nodes with stubs. *IEEE Transactions on Microwave Theory and Techniques* 1995; **43**(2):452–456.
13. Huber C, Krumpholz M, Russer P. Dispersion in anisotropy media modeled by three-dimensional TLM. *IEEE Transactions on Microwave Theory and Techniques* 1995; **43**(8):1923–1934.
14. Krumpholz M, Russer P. A generalized method for the calculation of TLM dispersion relations. *Proceedings of the 23th EMC*, Madrid, Spain, 1993; 288–291.
15. Russer P, Krumpholz M. The Hilbert space formulation of the TLM method. *International Journal of Numerical Modeling*: *Electronic Network*, *Devices and Fields* 1993; **6**(1):29–45.
16. Krumpholz M, Russer P. Two dimensional FDTD and TLM. *International Journal of Numerical Modeling*: *Electronic Network*, *Devices and Fields* 1994; **7**(2):141–153.
17. Krumpholz M, Russer P. A field theoretical derivation of TLM. *IEEE Transactions on Microwave Theory and Techniques* 1994; **42**(9):1660–1668.
18. Hein S. Finite difference time domain approximation of Maxwell's equations with non-orthogonal condensed TLM mesh. *International Journal of Numerical Modeling*: *Electronic Network*, *Devices and Fields* 1994; **7**:179–188.
19. Hein S. Synthesis of TLM algorithms in the propagator integral framework. *Proceedings of the 2nd International Workshop on Transmission Line Matrix (TLM) Modeling—Theory and Applications*, Munich, Germany, 1994; 1–11.
20. Trenkic V, Christopoulos C, Benson TM. Development of a general symmetrical condensed node for the TLM method. *IEEE Transactions on Microwave Theory and Techniques* 1996; **44**(12):2129–2135.
21. Trenkic V. Development and characterization of advanced nodes for the TLM method. *Ph.D. Thesis*, University of Nottingham, U.K., 1995.